International Symposium
On Turbulence and Shear Flow
Phenomena (TSFP-8)
August 28 - 30, 2013 Poitiers, France

PARTICLE DISPERSION IN FLOWS OVER ROUGH SURFACES

David Sassun
Dipartimento di Meccanica e Aerospaziale
Università di Roma "La Sapienza"
Via Eudossiana 16, Roma (Italy)
david.sassun@uniroma1.it

Paolo Orlandi
Dipartimento di Meccanica e Aerospaziale
Università di Roma "La Sapienza"
Via Eudossiana 16, Roma (Italy)

Matteo Bernardini
Dipartimento di Meccanica e Aerospaziale
Università di Roma "La Sapienza"
Via Eudossiana 16, Roma (Italy)

Sergio Pirozzoli
Dipartimento di Meccanica e Aerospaziale
Università di Roma "La Sapienza"
Via Eudossiana 16, Roma (Italy)

Abstract

The dispersion of particles in turbulent flows is a very common, yet not fully understood problem. In this work we deal with a fully developed turbulent channel flow, at $Re_\tau = 180$. The influence of wall roughness on the velocity field and on the particle dispersion is analysed. Three types of surface are studied: a smooth wall, a series of staggered cubes and triangular riblets parallel to the flow direction. The cubes strongly increase the pressure gradient necessary to maintain a constant mass flow rate, whereas the riblets yield drag reduction with respect to the smooth channel case. The particle statistics are analysed in terms of their mean square separation, for which a theoretical reference is provided by the Richardson law, which applies to isotropic turbulence. Significant deviations are found in the channel flow, dependent on the type of roughness, the Stokes number and the initial position of dispersion.

1 Introduction

Particle transportation and deposition are important in a wide range of applications, involving a number of different disciplines. Typical examples range from sediment transportation in rivers to dispersion of scalars in physiological flows, deposition of droplets in steam turbines and dispersion of pollutants in the atmosphere. It is interesting to estimate how the dispersion of particles is affected by a solid surface, as it occurs in channel and pipe flows, because of the simpler nature of these problems. There are several studies analysing particle motion in wall turbulence, both experimental and numerical. Most of the computational analyses focus on the near wall region and its structures (Guha (2008), Kaftori et al. (1995), Marchioli et al. (2003), Pan et al. (1996)), but there have also been efforts to understand the effect of the large-scale motions (Bernardini et al. (2012)). These studies deal with perfectly smooth walls, although this condition is rarely achieved in practical applications. Turbulent flows over rough walls have been studied extensively (Jiménez (2004)), but the description of the dispersion of particles over this kind of surface is still lacking.

Real surface roughness is random in nature but, in order to study the effects on the flow, it is useful to understand the effects of regular geometries, such as bars or three dimensional elements. The former can be oriented either transverse to the stream direction, yielding drag increase, or parallel to the stream, yielding, in some cases, drag reduction (Orlandi and Leonardi (2006)). In the present study, three types of surfaces are analysed: the smooth channel for validation and reference, staggered cubes (3D) and riblets parallel to the flow direction (2D).

The DNS furnishes all the variables of interest at every point of the flow, including near to or between the roughness elements. An important quantity, difficult to measure close to the roughness in experiments, is the wall-normal Reynolds stress. This parameter is crucial in the transition from laminar to turbulent flow (Orlandi (2011)), and it is proportional to the roughness function (Orlandi and Leonardi (2006)), which is often used to quantify the effects of the roughness on the mean velocity profile.

The goal of this study is two-fold: i) study the influence of the roughness on the velocity field, and ii) analyse the relative dispersion of the particles. The latter goal is achieved primarily by examining the mean square separation of the particles, as a function of the initial distance from the wall, the direction of separation, the Stokes number and the type of roughness.

2 Physical and numerical model

2.1 Flow phase

The nondimensional incompressible Navier-Stokes equations, solved in this work, are:

$$\frac{\partial u_i}{\partial t} + \frac{\partial u_i u_j}{\partial x_j} = -\frac{\partial p}{\partial x_i} + \frac{1}{Re}\frac{\partial^2 u_i}{\partial x_j^2} + \Pi\delta_{1i}\,, \quad \frac{\partial u_i}{\partial x_i} = 0\,,$$

where Π is the pressure gradient required to maintain a constant mass flow rate, u_i is the component of the velocity vector in the i direction, and p is the pressure. This set of equations has been discretized in an orthogonal coordinate system, with a staggered second-order finite difference

method. The integration in time has been made with a third-order low storage Runge-Kutta algorithm, coupled with a second-order Crank-Nicolson scheme combined in the fractional step procedure. Further details are found in Orlandi (2000) and are not repeated here.

The interaction between the flow and the roughness is reproduced by the immersed boundary technique, which assumes that the velocity is zero inside the body, and applies a correction to the viscous term at the first grid point near the solid surface. This method is described in detail in Orlandi and Leonardi (2006).

2.2 Particles phase

The Lagrangian frame of reference is the most natural one to deal with the dispersion of particles in a fluid, therefore the Lagrangian Particle Tracking is used. Under the assumption of one-way coupling, point-wise, spherical and neutrally buoyant elements, the only force applied is the Stokes drag, and the equations of motion of solid particles are:

$$\frac{dx_p}{dt} = u_p$$

$$\frac{du_p}{dt} = \frac{c_D}{\tau_p}\left(u - u_p\right)$$

where x_p and u_p are the position and the velocity of the particles, u is the velocity of the fluid at the particle position, $\tau_p = \frac{\rho_p d_p^2}{18\mu}$ is the particle relaxation time, and the Stokes drag coefficient is corrected with the empirical law (Schiller and Naumann (1935)) $c_D = 1 + 0.15 Re_p^{0.687}$, when the particle Reynolds number $Re_p = d_p \frac{|u-u_p|}{\nu}$ does not comply with the Stokes flow condition (small Re_p). The particle relaxation time is made dimensionless dividing by the viscous time scale, to obtain the Stokes number $St = \tau_p u_\tau^2/\nu$.

Periodicity conditions for the flow in the x and z directions imply that particles exiting from one side re-enter in the opposite. It is assumed that when a particle hits a wall, it is absorbed there. At the beginning of the simulation, a null velocity has been imposed to the particles, which for $St = 0$ immediately becomes equal to that of the fluid.

The motion of the particles is solved by using the flow velocity stored at equal time intervals. It has been verified that the results are not influenced by this time interval.

2.3 Setup

Three types of surfaces have been analysed: a smooth channel (hereinafter referred to as C), staggered rows of prisms (P, Fig. 1a) and triangular riblets aligned with the flow (T, Fig. 1b). The roughness is located on the lower wall ($-1.2 < y < -1$), while on the upper wall the surface is smooth. The other dimensions of the computational domain are $L_x = 8$ in the stream-wise direction and $L_z = 4$ in the span-wise direction.

All the simulations are performed at $Re = \frac{uh}{\nu} = 4200$ ($Re_b = 2800$) corresponding to a smooth channel with $Re_\tau = 180$. The different values of Re_τ on the channel walls are given in Table 1. For the three-dimensional square cubes, $k = 0.2$ corresponds to $k^+ = 36$, therefore the surface can be considered fully rough (Jiménez (2004)).

This study deals with inertial particles ($St = 25$) and tracers ($St = 0$). The particles are located at $t = 0$ on different planes ($y_0^+ = 2$ and centreline), with random x and z coordinates. All simulations are performed with 40000 particles. The elements are coupled, and each pair has an initial distance $d_0 = 0.0043714$, parallel to the Cartesian axes. The distance between three sets of 10000 couples is oriented in the x, y and z directions (referred to as $d_{0,x}$, $d_{0,y}$ and $d_{0,z}$). Statistics are acquired separately over these different sets. The initial distance and planes where the particles are located match those of Pitton et al. (2012), in order to validate our simulation for the smooth channel.

Table 1. Friction velocities and Reynolds numbers at the lower and upper walls, and percent difference of the mean pressure gradient, compared to that of the smooth channel

	$u_{\tau,l}$	$u_{\tau,u}$	$Re_{\tau,l}$	$Re_{\tau,u}$	$\frac{\overline{\Pi}_i - \overline{\Pi}_C}{\overline{\Pi}_C}$
C	0.0419	0.0420	176.1	176.1	0
P	0.0451	0.0704	189.5	295.9	0.854
T	0.0409	0.0388	171.8	162.8	-0.137

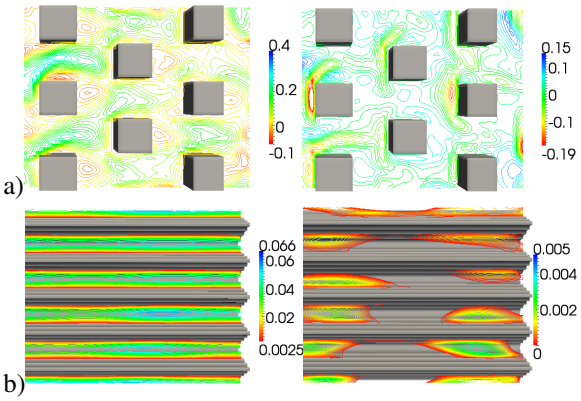

Figure 1. Contour plots of u (left) and v (right) at $y = -1.1$ (half the height of the obstacles), superimposed on the roughness elements, for a small portion of the domain; a) P; b) T

3 Results

Table 1 indicates an increase of the requested pressure gradient of about 85% with respect to that of a smooth channel for 3D obstacles, and a reduction of about 14% for the riblets. The drag components, computed from the Navier-Stokes equation in the x direction (not shown), can explain this behaviour. In the smooth channel, the viscous drag is the same for both walls, the form drag and the drag due to the non-linear terms are negligible, as expected. In P, the viscous drag decreases on the lower wall, and the form drag is the major component. This is also the term that causes the oscillatory trend in time for Π, which is an indication of greater turbulent activity and has been linked to an increase in the frequency of the bursting. In T, a weak form drag is present, and the viscous drag on the rough wall is lower: although the wetted surface is larger, the shear stresses are lower. This is because the shear stress is proportional to the velocity gradient in the wall normal direction, which are smoother than in the plane channel case.

The time evolution of the average square distance of the pairs is analysed and the differences with the Richardson law (Richardson (1926)) $\left\langle d^2(t)\right\rangle = C_2 \varepsilon t^3$, valid for isotropic turbulence in the presence of significant scale sep-

aration, are shown. It is expected that the shear induced by the wall affects the dispersion, causing higher rates of separation, when the distance becomes comparable with the integral scale of the flow. The exponent of the resulting power law is also dependent on the distance from the wall.

The results have been validated with those of Pitton et al. (2012). Fig. 2a shows that the dispersion is little affected by the initial orientation when the particles are released on the centreline. A t^6 power law is found in this case, showing that the mean shear causes a significant deviation from the isotropic turbulence in this zone. Fig. 2b on the other hand highlights that the orientation is important near the wall. In this region, the highest dispersion is achieved when the particles are slightly separated in the wall-normal direction, because of the sharper velocity gradient. In this case, the Richardson law is recovered for long times, while a power law t^2 is found for small separations. There is also a significant anticipation of the rise of the curve, with respect to the $y_0 = 0$ case. This is because the velocity differential are much sharper, and even a small distance can cause the particles to move apart from one another almost as soon as they are released. Despite having the same distance from the wall, the mean separation is higher in the $d_{0,z}$ case than in $d_{0,x}$. In these cases, the separation is very fast, reaching a t^8 slope. The reason of this behaviour is due to the effects of the alternation of low and high speed zones. The reduced velocity gradient in the x direction explains the reduction of the particle dispersion. The contour plot of the velocity field at the end of the simulation (Fig. 6a-b) shows the real position of the particles, i.e. the x coordinate is not constrained in $[0, 8]$, in order to visualize only those in the $0 < x < 16$ region. The particles tend to cluster near or around the low speed streaks, and to avoid the higher velocity zones . The transverse sections show that the particles released on the centreline achieve a homogeneous distribution throughout the whole domain, but when released near the wall, they cluster inside the streaks (Fig. 5a-c). For long times, the three curves tend to collapse, showing that even in the $y_0^+ = 2$ case the global shear becomes predominant at high separations, independently from the initial orientation of the distance. As said, the Richardson law is recovered for all three initial orientations.

The results of the rough wall simulations are shown in Fig. 3 for tracers. The charts at $y_0 = 0$ are not shown because they highlight the same trend discussed above, with a slight difference in the absolute values. The fact that the relative dispersion is not influenced by the roughness in the centre of the channel is a proof of the limited range of influence of the rough wall (Townsend's (1976) similarity hypothesis). When the particles are released near the wall, the initial orientation is less relevant than in C, implying that the flow is more isotropic in this region, for both P and T. The P flow, being the case with the greater turbulent activity, generates the highest dispersion. After 10 viscous time units, the separation in this case is larger than in the others (see Table 2 for a comparison). The only case in which it is lower is for inertial particles near the wall. The plot shows a delay of the separation, presumably resulting from the decrease in velocity caused by the three dimensional roughness. The collapse of the $d_{0,x}$ and $d_{0,z}$ curves in the graph can be explained with the absence of a velocity gradient in the span-wise direction. Flow visualizations of P (Fig. 6c-d) show the absence of streaks, which are the main cause for differential dispersion in the stream and span-wise directions. The transverse plane visualiza-

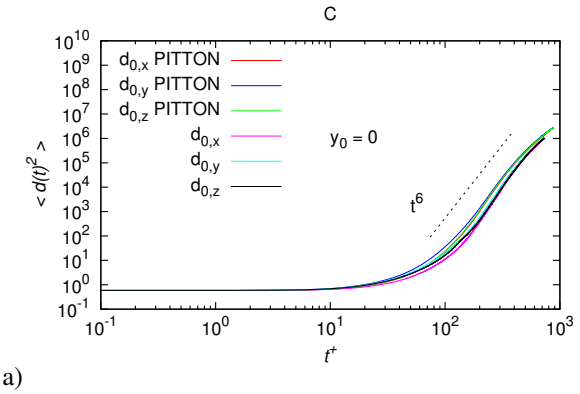

a)

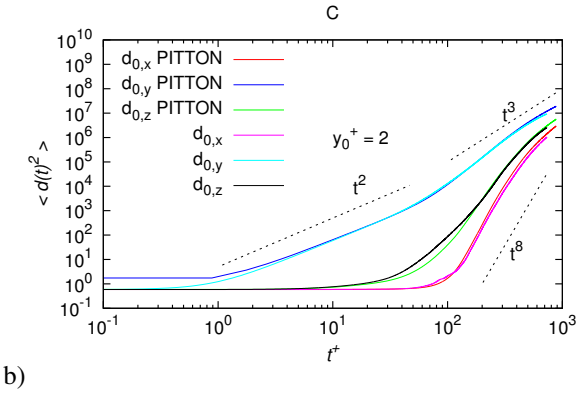

b)

Figure 2. Time evolution of the mean square separation for $St = 0$, for the smooth channel

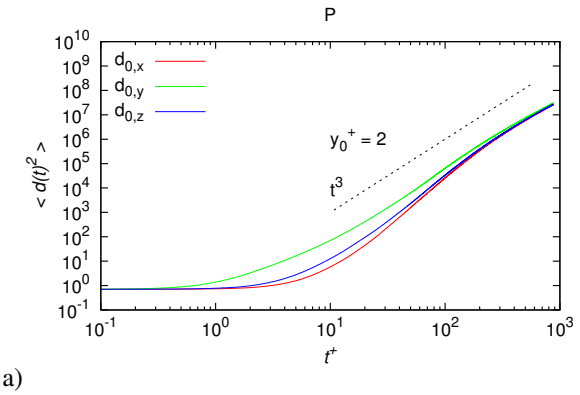

a)

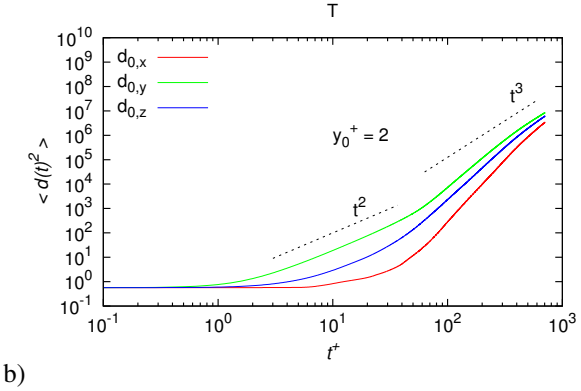

b)

Figure 3. Time evolution of the mean square separation for rough channels, $St = 0$; a) P, b) T

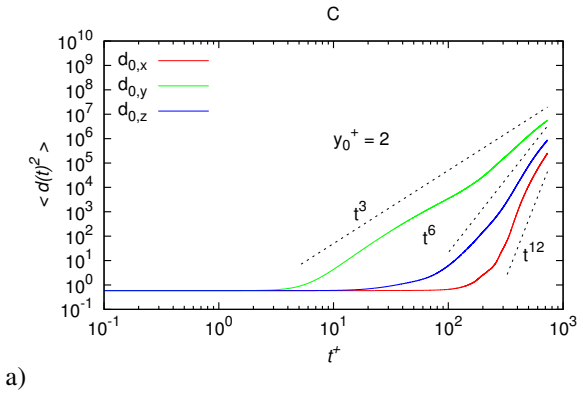

a)

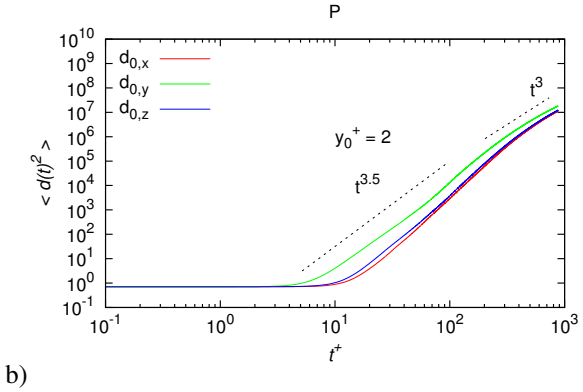

b)

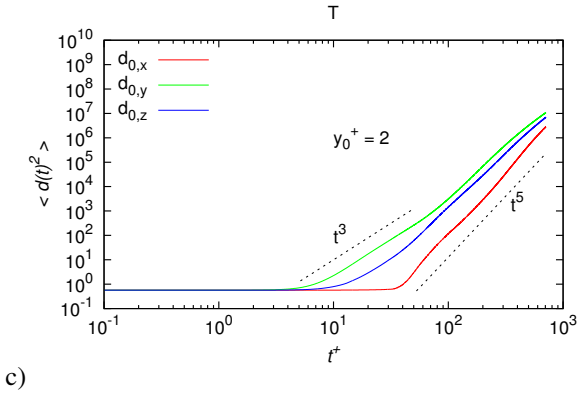

c)

Figure 4. Time evolution of the mean square separation for $St = 25$; a) C, b) P, c) T

tion (Fig. 5e) indicates that the particles are scattered in the channel more evenly than in the smooth case. In all three cases, a trend similar to the Richardson law is recovered, consistently with the previous finding of a better isotropy. In T, the same power law is maintained at large separations, with a more shallow slope in the initial transient. The influence of the initial orientation is less significant than in the smooth channel, but the profiles do not overlap as in P, since there is still a velocity gradient in the span-wise direction. Fig. 6e-f shows the presence of fluid structures similar to the streaks in the smooth channel. Since they are a result of the varying distance from the boundary where the no-slip condition is applied, the effect is reduced to obtain something in between the two previous cases. However, as seen in the transverse plane (Fig. 5g), the resulting particle clusters are not caused by these structures, but by the boundary itself: the particles arrange themselves around the riblets, but no significant cluster is formed in the flow over the roughness elements. The asymptotic behaviour shows a

Table 2. Mean square separation $\left\langle d(t)^2 \right\rangle$ at $t^+ = 10$

	$St = 0$		$St = 25$	
	$y_0 = 0$	$y_0^+ = 0$	$y_0 = 0$	$y_0^+ = 0$
C	0.696	59.98	0.595	4.398
P	1.130	71.52	0.726	4.111
T	0.657	19.19	0.574	2.283

t^3 slope, consistent with the other cases. This would suggest an independence of the dispersion from the type of surface for long times. The particle couples that contribute the most in this interval are those that were able to escape the near-wall region. This is consistent with the notion of the limited range of influence of the surface on the overlying velocity field.

Fig. 4 illustrates the time evolution of the distance of the inertial particles released near the wall. As seen in the $St = 0$ case, there is a significant difference in C between the initial orientation cases. The delay experienced by the particles separated in the wall-parallel direction causes the curves to be even steeper. The same happens in the rough cases: the growth is delayed and the resulting power laws show an increase of the exponents. Figs. 5b-d show the effect of the Stokes number. When $y_0 = 0$, the only difference is the higher segregation but, in the $y_0^+ = 2$ case, there is also a lower dispersion towards the centre of the channel. In P (Fig. 5f), most particles settle on the roughness elements, and the few that escape the near-wall region are dispersed uniformly in the domain. T shows a different behaviour (Fig. 5h): as in the previous case, most particles are deposited on the wall, but the velocity field is unable to diffuse the others efficiently, resulting in a higher concentration in the lower half of the channel.

4 Conclusions

In this study the effect of wall roughness on the particle dispersion is analysed. Three different walls are studied: a smooth surface, staggered cubes and triangular riblets aligned with the flow. It is found that the direction of the initial separation between particle pairs is most important near the wall. Because of the near isotropy achieved in the centre, the difference regarding this parameter is negligible. This provides additional evidence to the fact that the wall roughness influence is limited to the near-wall region. In the smooth wall case, the cause of this behaviour are the sharp velocity gradients in the y direction and the low speed streaks, which generate a velocity differential in the span-wise direction as well. The particles tend to remain trapped in the streaks generating small clusters. The absence of these near-wall structures and the more isotropic nature of the flow cause a near collapse of the profiles in the three-dimensional roughness case. With this geometric configuration, the average dispersion is higher than for the smooth channel, and the particles are more evenly distributed. The triangular riblets are somewhere in between: above the roughness elements, alternate streaks of low and high speed fluid are generated, but the resulting clustering of particles is not affected by these weak structures. The particles are concentrated between the roughness elements,

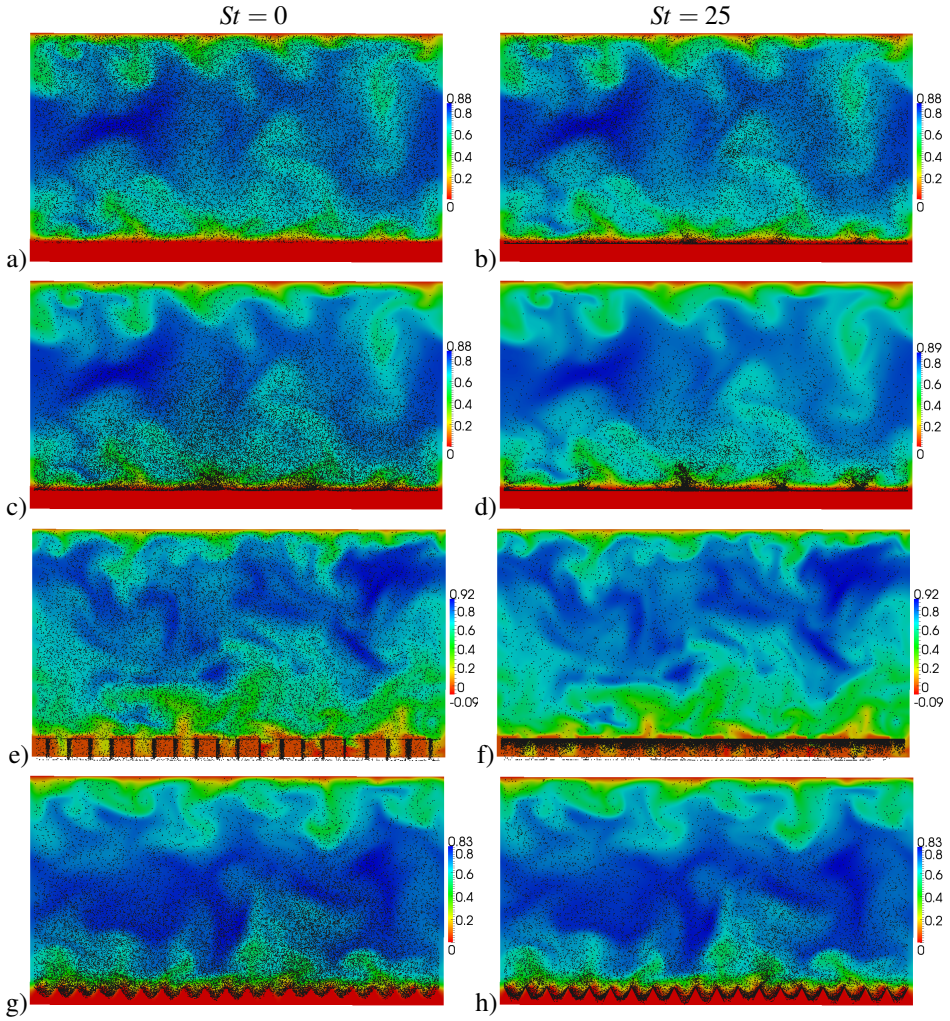

Figure 5. Final position of the particles superimposed on the stream-wise velocity at the $x = 0$ section. a) C: $St = 0$, $y_0 = 0$; b) C: $St = 25$, $y_0 = 0$; c) C: $St = 0$, $y_0^+ = 2$; d) C: $St = 25$, $y_0^+ = 2$; e) P: $St = 0$, $y_0^+ = 2$; f) P: $St = 25$, $y_0^+ = 2$; g) T: $St = 0$, $y_0^+ = 2$; h) T: $St = 25$, $y_0^+ = 2$

and fail to reach a homogeneous distribution in the rest of the domain.

The Stokes number has a marginal effect on the mean square separation: it causes a lower average value, but the same trends as in the tracers simulations are recovered. As expected, the deposition rates increase significantly, and the overall dispersion is reduced. The roughness effect is also highlighted: in C, the segregation in the streaks is clearer than in the tracers cases while, in P and in T, more particles settle on the obstacles or remain segregated in the near-wall region.

References

[1] Bernardini M., Pirozzoli S., Orlandi P. (2012), "Large-scale influences on particle dispersion in wall-bounded flows", submitted to International Journal of Multiphase Flow

[2] Guha A. (2008), "Transport and deposition of particles in turbulent and laminar flow", Annual Review of Fluid Mechanics, vol. 40

[3] Jiménez J. (2004), "Turbulent flows over rough walls", Annual Review of Fluid Mechanics, vol. 36

[4] Kaftori D., Hetsroni G., Banerjee S. (1995), "Particle behavior in the turbulent boundary layer. i motion, deposition and entrainment", Physics of Fluids, vol. 7

[5] Marchioli C., Giusti A., Salvetti M., Soldati A. (2003), "Direct numerical simulation of particle wall transfer and deposition in upward turbulent pipe flow", International Journal of Multiphase Flow, vol. 29

[6] Orlandi P. (2000), "Fluid Flow Phenomena - A Numerical Toolkit", Kluwer Academic Publisher

[7] Orlandi, P., Leonardi, S. (2006), "DNS of turbulent channel flows with two- and three-dimensional roughness", Journal of Turbulence, vol. 7

[8] Orlandi P. (2011), "DNS of transitional rough channels", Journal of Turbulence, vol. 12

[9] Pan Y., Banerjee S. (1996), "Numerical simulation of particles interactions with wall turbulence", Physics of Fluids, vol. 8

[10] Pitton E., Marchioli C., Lavezzo V., Soldati A., Toschi F. (2012), "Anisotropy in pair dispersion of inertial particles in turbulent channel flow", Physics of Fluids, vol. 24

[11] Richardson L. F. (1926), "Atmospheric diffusion shown on a distance-neighbour graph", Proceedings of the Royal Society A, 110

[12] Schiller L., Naumann A. (1935), "A drag coefficient correlation", Z. Ver. Deutsch. Ing., 77

[13] Townsend A. A. (1976), "The Structure of Turbulent Shear Flows", Cambridge University Press

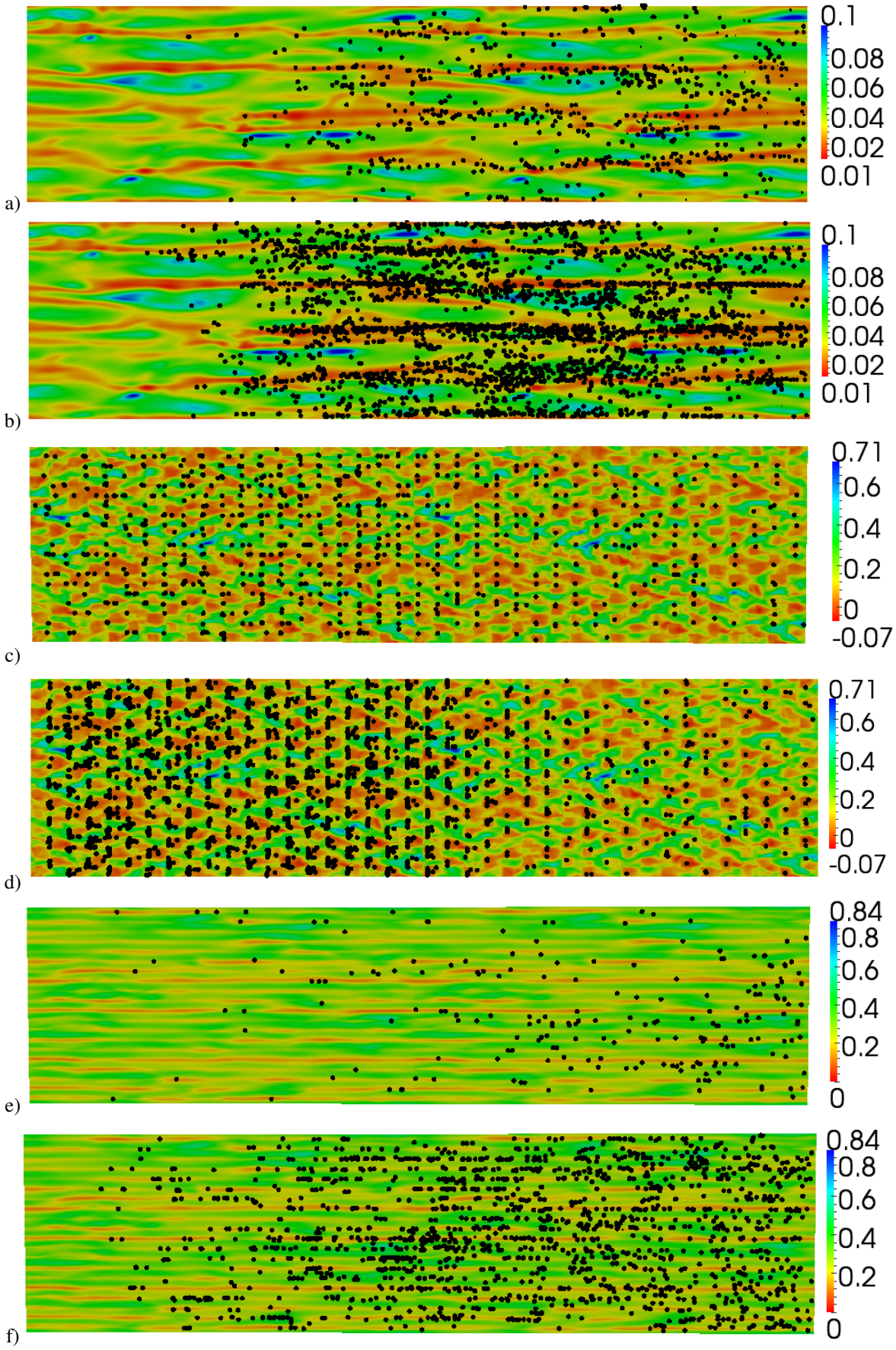

Figure 6. Final positions of the particles in $0 < x < 16$, superimposed on a xz section at $y = -0.99$ of the last velocity field; a) C: $St = 0$; b) C: $St = 25$; c) P: $St = 0$; d) P: $St = 25$; e) T: $St = 0$; f) T: $St = 25$